Supporting Information

Cote et al. 10.1073/pnas.1013674107

SI Text

1. Accuracy of Rotational Correlation Function (RCF) from a Finite Molecular Dynamics (MD) Trajectory (Fig. S4). For free diffusion (corresponding to an exponential decay of the RCF, $\alpha_n = 1$), the accuracy of an RCF is severely limited by the finite duration of the trajectory simulated (1, 2). To evaluate the accuracy of an RCF computed for a finite trajectory, we first computed $\bar{T}_1$ and $\bar{T}_2$ from simulated trajectories of a free 1D normal Brownian motion using Eq. **2** of the main text and compared the numerical results to the exact analytical RCF. The RCFs computed numerically were very accurate only up to about 1% of the duration of the trajectory because, at longer times, the statistics for the initial conditions t' in Eq. **2** of the main text were incomplete, and spurious oscillations of the RCF occur although the decay of the RCF was reproduced very qualitatively, in agreement with ref. 2. By extrapolating these results to an RCF computed from MD, the RCF $\bar{T}_2$ and $\bar{P}_2$ computed from a trajectory of 80 ns (duration used in the present work) should be very accurate only up to about 1 ns.

For most of the residues along the sequence of the amino acids, the RCF of the dihedral angles γ and of the N-H bonds computed from an MD trajectory of 80 ns converge to a plateau value on the 1-ns time scale and are therefore accurately described, as for γ_{11} and γ_{20} in Fig. S4*a* and for $(\text{N-H})_{11}$, $(\text{N-H})_{20}$, and $(\text{N-H})_{35}$ in Fig. S4*b*. Noisy oscillations were found at about $t > 2$ ns for some RCFs that do not converge to a plateau on the nanosecond time scale as shown, for example, for γ_{35} and γ_{39} in Fig. S4*a* and for $(\text{N-H})_{39}$ in Fig. S4*b*. The oscillations are due to insufficient sampling of the long-time fluctuations of γ and N-H bonds ($t \gg 1$ ns) of these residues on the duration of the MD trajectories. For the coarse-grained dihedral angles, nonmonotonic behavior of the RCF occurs, in particular, for dihedral angles with multiple-minima free-energy profiles (FEPs) (as for γ_{35} and γ_{39} in Fig. S4*a*). As shown previously (3), the transitions between different minima of $V(\gamma)$ are rare events on the time scale of the duration of the present MD trajectories (80 ns) and are thus responsible for a nonmonotonic behavior of the long-time mean-square displacement (MSD) (see figure 2 in ref. 3) and RCF of these dihedral angles. The RCF of N-H bonds and of dihedral angles behave similarly: Backbone amide N-H bonds of residues corresponding to the virtual bonds forming the dihedral angles with multiple-minima FEP are also inaccurate at long time; i.e., ($t \gg 1$ ns) [as, for example, $(\text{N-H})_{39}$ in Fig. S4*b*].

Finally, it should be mentioned that, to extract the type of behavior of an RCF, one needs to fit the RCF to at least one decade of time (2, 4). Consequently, to improve the accuracy of the RCF of γ and N-H bonds shown in Fig. S4, up to 10 ns would require MD runs of 1 μs long and extensive computational resources. Because NMR relaxation probes subnanosecond and nanosecond motions and we, therefore, extracted the parameters α and D_α from RCF computed up to 1 ns, this was not necessary as the inaccuracies of some RCFs occur at about $t > 2$ ns and do not affect our conclusions.

2. Comparison of Values of α and D_α Extracted from RCFs up to 50 ps and 1 ns. ***2.1. Dihedral angles (Fig. S5 b and c)*** The values of the exponent α and of the diffusion constant D_α extracted from a fit of the RCF up to 50 ps by using a stretched exponential were compared to the values of these quantities computed independently by fitting the MSD(t) of each angle γ_n by $2D_\alpha t^\alpha$ for $t < 50$ ps. The exponents and diffusion constants computed from the MSD were in excellent agreement with those deduced from the RCF, as shown in Fig. S5 *b* and *c*. However, some deviations are observed for the exponents of residues 35 to 39 (Fig. S5*c*), which have pronounced anharmonic free-energy profiles (Fig. S3). For example, the value of the exponent of γ_{37} extracted from $\bar{T}_2$ by fitting the RCF by a stretched exponential was $\alpha = 0.22$, whereas the value deduced from its MSD was $\alpha = 0.24$.

The values of D_α computed by fitting the RCF by a stretched exponential up to 1 ns (empty triangles) are close to the values obtained by fitting the RCF up to 50 ps (filled diamonds, superposed to the filled squares) except for a few residues ($n = 5, 6, 38$, and 40) (Fig. S5*b*). The quantity $2D_\alpha$ is the variance of the distribution of the angular steps of the dihedral angles moving each picosecond (3) and is not expected to vary so much with the time scale. The values of α computed by fitting the RCF by a stretched exponential up to 1 ns (empty triangles) are, in general, lower than the values obtained by fitting the RCF up to 50 ps (filled diamonds, superposed to the filled squares) with a few exceptions ($n = 3, 26, 33$, and 39) (Fig. S5*c*). A variation of the exponent of the RCF as a function of the time scale considered is expected and reflects the fact that the RCF of most of the dihedral angles γ are decaying functions on the 50-ps time scale and converge to a plateau (corresponding to $\alpha = 0$) on the 1-ns time scale.

2.2. N-H bonds (Fig. S6 b and c). The values of the exponent α and of the diffusion constant D_α extracted from a fit of the RCF up to 50 ps by using a stretched exponential were compared to the values of these quantities computed independently by fitting the MSD(t) of each N-H bond by $4D_\alpha t^\alpha$ for $t < 50$ ps. The diffusion constants computed from the MSD were in excellent agreement with those deduced from the RCF, as shown in Fig. S6*b* (a small deviation is observed only for residues 30 and 37). The exponents (Fig. S6*c*) computed independently from the MSD and extracted from the stretched exponential fitted to the RCF up to 50 ps agree for most of the residues. Deviations are observed for the exponents of residues 21, 37, 38, and 40, which have anharmonic free-energy profiles.

As found for the dihedral angles γ, the values of D_α computed by fitting the RCF by a stretched exponential up to 1 ns (empty triangles) are extremely close to the values obtained by fitting the RCF up to 50 ps (filled diamonds, superposed to the filled squares for most of the residues) except for few residues ($n = 9, 20, 21, 38, 40, 42$, and 43). The values of α computed by fitting the RCF by a stretched exponential up to 1 ns (empty triangles) are in general lower than the values obtained by fitting the RCF up to 50 ps (filled diamonds, superposed to the filled squares for most of the residues) with a few exceptions ($n = 26, 27, 28$, and 37). As for the dihedral angles γ, the variation of the exponents reflects the convergence of most of the RCFs to a plateau on 1-ns time scale, whereas they are a decaying function on the 50-ps time scale.

3. Relation Between RCF and MSD at Short Time (Demonstration of Eq. 1 of Main Text). ***3.1. Diffusion on a circle.*** Fluctuations of each coarse-grained dihedral angle γ are represented by the stochastic rotations of a vector $\boldsymbol{u}$ defining the position of a random walker on the unit circle (the subscript n is omitted in the notations for clarity). Indeed, at each time t, for each dihedral angle γ, one may define a unit vector by $\mathbf{u}(t) \equiv \{\cos[\gamma(t)], \sin[\gamma(t)]\}$. The motion of this 2D unit vector is thus in a plane and describes the stochastic motion of a point on a circle. The concept of Brownian motion on a circle can also be understood as follows: The angle γ_n is the angle between two planes, so the fluctuations of γ_n correspond

indeed to a stochastic motion on a circle perpendicular to the bond $C^{\alpha}(n)$-$C^{\alpha}(n+1)$.

The scalar product $x(t';t'+t) \equiv \boldsymbol{u}(t') \bullet \boldsymbol{u}(t'+t)$ is the cosine of the angular displacement $\Delta\gamma(t';t'+t)$ of $\boldsymbol{u}$ between t' and $t'+t$ and $-\pi \le \Delta\gamma(t';t'+t) \le \pi$. In this representation, the RCFs of $\Delta\gamma$ are those of a random walk on a circle, which are the time (or ensemble) averages of Tchebychev polynomials (see ref. 5):

$$\tilde{T}_l(t) = \langle \cos[l\Delta\gamma(t';t'+t)] \rangle_{t'} = C_l(t), \qquad \textbf{[S1]}$$

where the average in Eq. **S1** is over all initial orientations of $\boldsymbol{u}$ (all t'). For $\tilde{T}_1$ and $\tilde{T}_2$ analyzed in the main text, it is found from Eq. **S1** that

$$\tilde{T}_1(t) = \langle \cos[\Delta\gamma(t';t'+t)] \rangle_{t'}, \qquad \textbf{[S2]}$$

$$\tilde{T}_2(t) = 2\langle \cos^2[\Delta\gamma(t';t'+t)] \rangle_{t'} - 1. \qquad \textbf{[S3]}$$

For short times t, the most probable displacements $\Delta\gamma$ are small [see the equation of the probability density function (PDF), $F(\Delta\gamma,t)$ of Eq. **S17** and Fig. S8 *g–j*] and, using the second order expansion of $\cos(\Delta\gamma) \approx 1 - (\Delta\gamma)^2/2$, it is found from Eqs. **S2** and **S3** that

$$\tilde{T}_1(t) \approx 1 - \frac{\mathrm{MSD}(t)}{2}, \qquad \textbf{[S4]}$$

$$\tilde{T}_2(t) \approx 1 - 2\mathrm{MSD}(t), \qquad \textbf{[S5]}$$

where the MSD of the dihedral angles is defined as usual:

$$\mathrm{MSD}(t) \equiv \langle [\Delta\gamma(t';t'+t)]^2 \rangle_{t'}. \qquad \textbf{[S6]}$$

Comparing Eqs. **S4** and **S5** with Eq. **1** of the main text, it is found that $K_1 = 1/2$ for $\tilde{T}_1$ and $K_2 = 2$ for $\tilde{T}_2$, as announced in the main text.

3.2. Diffusion on a sphere. Fluctuations of each $(\text{N-H})_n$ (Fig. S1) (except for PRO residues) are represented by the stochastic rotations of a vector $\boldsymbol{u}$ defining the position of a random walker on the unit sphere (the subscript n is omitted in the notations for clarity). Indeed, as each N-H bond is rotating in the 3D space, its *direction* (defined by a unit vector $\mathbf{u}$) defines the position of a point moving on a sphere in 3D.

The scalar product $x(t';t'+t) \equiv \boldsymbol{u}(t') \bullet \boldsymbol{u}(t'+t)$ is the cosine of the angular displacement $\Delta\xi(t';t'+t)$ of $\boldsymbol{u}$ between t' and $t'+t$. It is worth noting that, whereas $\Delta\gamma$ represents a one-dimensional displacement (on a circle), $\Delta\xi$ represents a two-dimensional angular displacement (on the surface of a sphere). The RCFs of $\Delta\xi$ are those of a random walk on a sphere, which are time (or ensemble) averages of the Legendre polynomials $P_l(t)$ (see ref. 5).

For $\tilde{P}_1$ and $\tilde{P}_2$, analyzed in the main text, they are given by

$$\tilde{P}_1(t) = \langle \cos[\Delta\xi(t';t'+t)] \rangle_{t'}, \qquad \textbf{[S7]}$$

$$\tilde{P}_2(t) = \frac{1}{2}[3\langle \cos^2[\Delta\xi(t';t'+t)] \rangle_{t'} - 1]. \qquad \textbf{[S8]}$$

For short times t, the most probable displacements $\Delta\xi$ are around 10° (see Fig. 2 of the main text, and Eqs. **S24** and **S26**). Using the second-order expansion of $\cos(\Delta\xi) = 1 - [\Delta\xi]^2/2$, it is found from Eq. **S7** and Eq. **S8** that

$$\tilde{P}_1(t) \approx 1 - \frac{\mathrm{MSD}(t)}{2}, \qquad \textbf{[S9]}$$

$$\tilde{P}_2(t) \approx 1 - \frac{3}{2}\mathrm{MSD}(t), \qquad \textbf{[S10]}$$

where the MSD was defined as usual:

$$\mathrm{MSD}(t) \equiv \langle [\Delta\xi(t';t'+t)]^2 \rangle_{t'}. \qquad \textbf{[S11]}$$

Comparing Eqs. **S9** and **S10** with Eq. **1** of the main text, it is found that $K_1 = 1/2$ for $\tilde{P}_1$ and $K_2 = 3/2$ for $\tilde{P}_2$ as announced in the main text.

4. PDF and RCF of Rotational Diffusion with a Time-Dependent Diffusion Coefficient. We demonstrate here that stretched exponentials are RCFs of rotational diffusion equations with an effective time-dependent diffusion coefficient $D(t) = \alpha D_{\alpha} t^{\alpha-1}$.

4.1. Useful properties of Tchebychev polynomials (ref. 6). The differential equation for Tchebychev polynomials is (see ref. 6)

$$\frac{\partial^2 T_l[\cos(\Delta\gamma)]}{\partial[\cos(\Delta\gamma)]^2}\sin^2(\Delta\gamma) - \cos(\Delta\gamma)\frac{\partial T_l[\cos(\Delta\gamma)]}{\partial[\cos(\Delta\gamma)]} = -l^2 T_l[\cos(\Delta\gamma)]. \qquad \textbf{[S12]}$$

Using the chain rule of derivatives, we find

$$\frac{\partial^2 T_l[\cos(\Delta\gamma)]}{\partial[\Delta\gamma]^2} = \frac{\partial^2 T_l[\cos(\Delta\gamma)]}{\partial[\cos(\Delta\gamma)]^2}\sin^2(\Delta\gamma) - \cos(\Delta\gamma)\frac{\partial T_l[\cos(\Delta\gamma)]}{\partial[\cos(\Delta\gamma)]}, \qquad \textbf{[S13]}$$

and we see that

$$\frac{\partial^2 T_l[\cos(\Delta\gamma)]}{\partial[\Delta\gamma]^2} = -l^2 T_l[\cos(\Delta\gamma)]. \qquad \textbf{[S14]}$$

4.2. Free diffusion on a circle (ref. 5). The equation for free diffusion of a walker on a circle is (see ref. 5)

$$\frac{\partial F(\Delta\gamma;t)}{\partial t} = D\frac{\partial^2 F(\Delta\gamma;t)}{\partial \Delta\gamma^2}, \qquad \textbf{[S15]}$$

where $F(\Delta\gamma;t)d\gamma$ is the probability that the vector $\boldsymbol{u}$, representing a dihedral angle γ (Fig. S1), is rotated by an angle $\Delta\gamma$ after a time $t > 0$ [with $F(\Delta\gamma;0) = \delta(\Delta\gamma)$]. We consider Eq. **S15** with a time-dependent diffusion coefficient, i.e.,

$$D \to D(t) = \alpha D_{\alpha} t^{\alpha-1}. \qquad \textbf{[S16]}$$

The solution of Eq. **S15** with $D(t)$ is

$$F(\Delta\gamma,t) = \frac{1}{2\pi} + \frac{1}{\pi}\sum_{l=1}^{\infty} \exp(-l^2 D_{\alpha} t^{\alpha}) T_l[\cos(\Delta\gamma)], \qquad \textbf{[S17]}$$

as is easily checked by using the property of Eq. **S14**. The constant $1/2\pi$ in Eq. **S17** ensures that F is normalized to 1. According to the ergodic hypothesis, the RCF (Eq. **2** of the main text) of a random walk on a circle can be computed from the PDF (Eq. **S17**):

$$C_l(t) \equiv \int_{-\pi}^{\pi} d\Delta\gamma T_l[\cos(\Delta\gamma)] F(\Delta\gamma;t). \qquad \textbf{[S18]}$$

By using Eq. **S17** in Eq. **S18** and the orthogonality of the Tchebychev polynomials (see ref. 6), it is found immediately that

$$C_l(t) = \tilde{T}_l(t) = \exp(-l^2 D_{\alpha} t^{\alpha}). \qquad \textbf{[S19]}$$

4.3. Useful properties of Legendre polynomials (ref. 6). The differential equation for Legendre polynomials is (see ref. 6)

$$\frac{\partial^2 P_l[\cos(\Delta\xi)]}{\partial[\cos(\Delta\xi)]^2}\sin^2(\Delta\xi) - 2\cos(\Delta\xi)\frac{\partial P_l[\cos(\Delta\xi)]}{\partial[\cos(\Delta\xi)]} = -l(l+1)P_l[\cos(\Delta\xi)]. \quad \text{[S20]}$$

Using the chain rule of derivatives, we find

$$\frac{\partial P_l[\cos(\Delta\xi)]}{\partial[\Delta\xi]} = -\frac{\partial P_l[\cos(\Delta\xi)]}{\partial[\cos(\Delta\xi)]}\sin(\Delta\xi),$$
$$\frac{\partial^2 P_l[\cos(\Delta\xi)]}{\partial[\Delta\xi]^2} = \frac{\partial^2 P_l[\cos(\Delta\xi)]}{\partial[\cos(\Delta\xi)]^2}\sin^2(\Delta\xi) - \cos(\Delta\xi)\frac{\partial P_l[\cos(\Delta\xi)]}{\partial[\cos(\Delta\xi)]}, \quad \text{[S21]}$$

and we obtain

$$\frac{\partial^2 P_l[\cos(\Delta\xi)]}{\partial[\Delta\xi]^2} + \cot(\Delta\xi)\frac{\partial P_l[\cos(\Delta\xi)]}{\partial[\Delta\xi]} = -l(l+1)P_l[\cos(\Delta\xi)]. \quad \text{[S22]}$$

4.4. Free diffusion on a sphere (ref. 5). The equation for free diffusion of a walker on a sphere is (see ref. 5)

$$\frac{\partial f(\Delta\xi;t)}{\partial t} = D\left[\frac{\partial^2 f(\Delta\xi;t)}{\partial\Delta\xi^2} + \cot(\Delta\xi)\frac{\partial f(\Delta\xi;t)}{\partial\Delta\xi}\right], \quad \text{[S23]}$$

where $f(\Delta\xi;t)$ is related to $F(\Delta\xi;t)$ by the following relation:

$$F(\Delta\xi;t) = 2\pi f(\Delta\xi;t)\sin(\Delta\xi). \quad \text{[S24]}$$

The quantity $F(\Delta\xi;t)d\xi$ is the probability that the vector $\boldsymbol{u}$, representing an N-H bond (Fig. S1), is rotated by an angle $\Delta\xi$ after a time $t > 0$ [with $f(\Delta\xi;0) = \delta(\Delta\xi)$]. Using Eq. **S24** in Eq. **S23**, we easily find the diffusion equation for F:

$$\frac{\partial F(\Delta\xi;t)}{\partial t} = D\left[\frac{\partial^2 F(\Delta\xi;t)}{\partial\Delta\xi^2} - \cot(\Delta\xi)\frac{\partial F(\Delta\xi;t)}{\partial\Delta\xi} + (\cot^2(\Delta\xi)+1)F(\Delta\xi;t)\right]. \quad \text{[S25]}$$

We consider Eq. **S23** with a time-dependent diffusion constant given by Eq. **S16**. The solution of Eq. **S23** with $D(t)$ is

$$f(\Delta\xi,t) = \frac{1}{4\pi} + \frac{1}{4\pi}\sum_{l=1}^{\infty}(2l+1)P_l[\cos(\Delta\xi)]\exp(-l(l+1)D_\alpha t^\alpha), \quad \text{[S26]}$$

as is easily checked by using the property Eq. **S22**. The constant $1/4\pi$ in Eq. **S26** ensures that F (Eq. **S24**) is normalized to 1. Using the ergodic hypothesis, the RCF (Eq. **3** of the main text) of a random walk on a sphere can be computed from the PDF (Eq. **S26**):

$$C_l(t) \equiv 2\pi\int_0^\pi d\Delta\xi\sin(\Delta\xi)P_l[\cos(\Delta\xi)]f(\Delta\xi;t), \quad \text{[S27]}$$

or using Eq. **S24**:

$$C_l(t) \equiv \int_0^\pi d\Delta\xi P_l[\cos(\Delta\xi)]F(\Delta\xi;t). \quad \text{[S28]}$$

By using Eq. **S26** in Eq. **S27** and the orthogonality of the Legendre polynomials (see ref. 6), it is found that

$$C_l(t) = \tilde{P}_l(t) = \exp[-l(l+1)D_\alpha t^\alpha]. \quad \text{[S29]}$$

4.5. PDF for a random walk on a circle as a sum of Gaussians. Following the arguments of Perrin (ref. 5), Eq. **S17** can be formulated alternatively as a sum of Gaussians:

$$P(\Delta\gamma,t) = \frac{1}{\sqrt{4D_\alpha\pi t^\alpha}}\sum_{k=-\infty}^{\infty}\exp\left(-\frac{(\Delta\gamma+2k\pi)^2}{4D_\alpha t^\alpha}\right). \quad \text{[S30]}$$

5. Derivation of the Scaling Property (Eq. 4 in the main text) for the PDF on a Circle. An approximate derivation of Eq. **4** for the PDF Eq. **S17** can be performed as follows: By assuming the rank l of the orthogonal polynomials to be a continuous variable, we may replace the sum in Eq. **S17** by an integral, i.e.,

$$F(\Delta\gamma,t) \approx \frac{1}{2\pi} + \frac{1}{\pi}\int_1^\infty dl\exp(-l^2D_\alpha t^\alpha)[\cos(l\Delta\gamma)], \quad \text{[S31]}$$

where, in addition, we used $T_l[\cos(\Delta\gamma)] = \cos(l\Delta\gamma)$ (see ref. 6). Applying the transformation $\Delta\gamma \to \Delta\gamma/h^{\alpha/2}$ to the right-hand side (rhs) of Eq. **S31**, we find that the right-hand side of Eq. **S31** is

$$\text{rhs} = \frac{1}{2\pi/h^{\alpha/2}} + \frac{1}{\pi}\int_1^\infty dl\exp(-l^2D_\alpha t^\alpha)\left[\cos\left(\frac{l}{h^{\alpha/2}}\Delta\gamma\right)\right]. \quad \text{[S32]}$$

By defining the variable $k = l/h^{\alpha/2}$, Eq. **S32** becomes

$$\text{rhs} = \frac{h^{\alpha/2}}{2\pi} + h^{\alpha/2}\frac{1}{\pi}\int_{1/h^{\alpha/2}}^\infty dk\exp[-k^2D_\alpha(ht)^\alpha][\cos(k\Delta\gamma)] \approx F(\Delta\gamma,ht)h^{\alpha/2}, \quad \text{[S33]}$$

where the last equality is deduced from Eq. **S31**. Eq. **S33** is the scaling property of Eq. **4** of the main text.

6. Numerical Test of the Scaling Property (Eq. 4 of the Main Text) for the PDF of the γ Dihedral Angles (Fig. S8 *g–j*). We discuss a numerical test of the scaling property (Eq. **4** of the main text) for $F(\Delta\gamma_n,t)$, i.e.,

$$F(\Delta\gamma_n,ht) = \frac{1}{h^{\alpha/2}}F\left(\frac{\Delta\gamma_n}{h^{\alpha/2}},t\right). \quad \text{[S34]}$$

Typical results, representative of the 215 PDFs $F(\Delta\gamma_n,t)$ computed for the 43 dihedral angles and the five MD trajectories, are shown in Fig. S8 for γ_{11} (with a harmonic FEP, Fig. S8 *g*, *Inset*, and *i*, *Inset*) and γ_{35} (with a multiple-minima FEP, Fig. S8 *h*, *Inset*, and *j*, *Inset*). For each of these dihedral angles, the PDF computed between 10 ps and 1 ns were first rescaled according to Eq. **S34** to the PDF computed at 100 ps (i.e., by choosing $h = 1$ in Eq. **S34** at $t = 100$ ps) with the values of $[\alpha,D_\alpha]$ at short time [calculated by fitting the RCF $\tilde{T}_2$ up to 50 ps (Fig. 1*A* of the main text)]. The results are shown in panels (*g*) and (*h*). There is a very good overlap between all PDFs for γ_{11} (panel *g*) and γ_{35} (panel *h*) but, because the parameters $[\alpha,D_\alpha]$ represent the decay of the RCF up to only 50–100 ps (Fig. 1*A* of the main text), small deviations are observed (Fig. S8 *g* and *h*) between the different PDFs at time $t > 100$ ps, which are due to the (small) variation of the exponent with time (as shown by the comparison of the two stretched exponentials in Fig. 1*C* of the main text). Indeed, for each dihedral angle, the PDFs computed between 10 ps and

1 ns were rescaled next according to Eq. **S34** to the PDF computed at 1 ns (i.e., by choosing $h = 1$ in Eq. **S34** at $t = 1$ ns) with the values of $[\alpha,D_\alpha]$ at long time (calculated by fitting the RCF $\tilde{T}_2$ up to 1 ns, Fig. 1*C* of the main text). The results are shown in Fig. S8 *i* and *j*. There is very good superposition of all PDFs at different times.

For dihedral angles with multiple-minima FEP, as for example γ_{35} (Fig. S8*h*), there is a deviation of the PDF from a pure Gaussian distribution (Fig. S8 *b* and *c* and *h* and *j*). Indeed, for dihedral angles with multiple-minima FEP (see Fig. S3), displacements $\Delta\gamma$ correspond both to fluctuations within a minimum of the FEP and to jumps ($\Delta\gamma > \Delta\gamma_i^*$ in Fig. S8 *h* and *j*) corresponding to transitions between different minima of the FEP.

7. Velocity–Velocity Correlation Function. The velocity–velocity correlation function (see ref. 7) $C_v(t)$ is defined by

$$C_v(t) = \left\langle \left[\frac{\partial\gamma(t+t')}{\partial t'}\right]\left[\frac{\partial\gamma(t')}{\partial t'}\right]\right\rangle_{t'}, \qquad \textbf{[S35]}$$

where the average is over all possible initial positions of $\boldsymbol{u}(t')$, i.e., all values of t'. At thermal equilibrium, the MSD(t) of the dihedral angles (Eq. **S6**) is related to $C_v(t)$ by an exact relation (see ref. 7):

$$\mathrm{MSD}(t) = 2t\left\{\int_0^t dt'\left(1-\frac{t'}{t}\right)C_v(t')\right\}. \qquad \textbf{[S36]}$$

By definition, the diffusion coefficient $D(t)$ is the term in braces in Eq. **S36**. At the limit $t \to \infty$, D is a constant:

$$D(\infty) = \int_0^\infty dt C_v(t). \qquad \textbf{[S37]}$$

Assuming a (slow) power-law decay of $C_v(t)$ with an exponent $\beta < 0$,

$$C_v(t) = A_\beta t^\beta, \qquad \textbf{[S38]}$$

we deduce for the term in braces in Eq. **S36**:

$$D(t) = \frac{A_\beta}{(\beta+1)(\beta+2)}t^{\beta+1}. \qquad \textbf{[S39]}$$

By comparing Eq. **S39** and the result $D(t) \approx \alpha D_\alpha t^{\alpha-1}$, we find that $\beta = \alpha - 2$ and finally,

$$C_v(t) \approx \alpha^2(\alpha-1)D_\alpha t^{\alpha-2}, \qquad \textbf{[S40]}$$

as stated in *Results and Discussion* in the main text. The power-law velocity correlation function given by Eq. **S40** implies that random Langevin forces are correlated in time (8) as found in fluorescence experiments by measuring the correlation function of the distance between two residues within a protein (9). It is worth noting that the rotational diffusion equation with a power-law diffusion coefficient, $D(t)$, is a simple physical model of the fluctuations of $\boldsymbol{u}_n$, which accounts for the anomalous diffusion (8). An exact (numerical) approach exists, which consists of solving the generalized Langevin equation (as in ref. 9) for each $\boldsymbol{u}_n$ in its own FEP, which is beyond the scope of the present work.

8. Exact Analytical Relations Between the FEP $V(\gamma)$ and $V(\theta,\varphi)$ and the Generalized Order Parameters S^2 of γ Dihedral Angles and N-H Bonds. The generalized order parameter S^2 is defined for the dihedral angles γ and, for the N-H bonds, as the limit at $t \to \infty$ of the RCF $\tilde{T}_2$ and $\tilde{P}_2$, respectively. It can be related exactly to the FEP by analytical relations as follows.

8.1. Diffusion on a circle (see Fig. S1). Using the following notations,

$$\mathbf{u} = (u_x,u_y) \equiv \mathbf{u}(t') = (\cos[\gamma(t')],\sin[\gamma(t')]) \qquad \textbf{[S41]}$$

and

$$\tilde{\mathbf{u}} = (\tilde{u}_x,\tilde{u}_y) \equiv \mathbf{u}(t'+\infty) = (\cos[\gamma(t'+\infty)],\sin[\gamma(t'+\infty)]), \qquad \textbf{[S42]}$$

the RCF (see Eq. **S3**) as $t \to \infty$ is

$$\tilde{T}_2(\infty) = 2\langle(\tilde{\mathbf{u}}\cdot\mathbf{u})^2\rangle - 1, \qquad \textbf{[S43]}$$

$$\tilde{T}_2(\infty) = 2\langle\tilde{u}_x{}^2u_x{}^2 + \tilde{u}_y{}^2u_y{}^2 + 2(\tilde{u}_x\tilde{u}_yu_xu_y)\rangle - 1, \qquad \textbf{[S44]}$$

in which the averages $\langle\,\rangle$ are over all the times (Eq. **S3**).

By definition, the vectors $\tilde{\mathbf{u}}$ and $\mathbf{u}$ are two orientations of the same vector separated by an infinite time. They are, therefore, statistically independent. Consequently, the average of their product is equal to the product of their averages. Using this property, we find

$$\tilde{T}_2(\infty) = 2[\langle\tilde{u}_x{}^2\rangle\langle u_x{}^2\rangle + \langle\tilde{u}_y{}^2\rangle\langle u_y{}^2\rangle + 2\langle\tilde{u}_x\tilde{u}_y\rangle\langle u_xu_y\rangle] - 1, \qquad \textbf{[S45]}$$

and

$$\tilde{T}_2(\infty) = 2[\langle u_x{}^2\rangle^2 + \langle u_y{}^2\rangle^2 + 2\langle u_xu_y\rangle^2] - 1. \qquad \textbf{[S46]}$$

In the derivation of Eq. **S46**, we used

$$\langle\tilde{u}_x{}^2(t')\rangle_{t'} = \langle u_x{}^2(t'+\infty)\rangle_{t'}, \qquad \textbf{[S47]}$$

$$\langle\tilde{u}_y{}^2(t')\rangle_{t'} = \langle u_y{}^2(t'+\infty)\rangle_{t'}, \qquad \textbf{[S48]}$$

$$\langle\tilde{u}_x(t')\tilde{u}_y(t')\rangle_{t'} = \langle u_x(t'+\infty)u_y(t'+\infty)\rangle_{t'}, \qquad \textbf{[S49]}$$

because a translation of the time scale by a constant ($+\infty$) does not change the averages.

Because $\mathbf{u}$ is a unit vector, one has

$$u_y{}^2 = 1 - u_x{}^2. \qquad \textbf{[S50]}$$

Using Eq. **S50** in Eq. **S46**, we find the following expression:

$$\tilde{T}_2(\infty) = 1 - 4\langle u_x{}^2\rangle + 4[\langle u_x{}^2\rangle^2 + \langle u_xu_y\rangle^2]. \qquad \textbf{[S51]}$$

Finally, using the relation **S41**, one finds

$$\tilde{T}_2(\infty) = 1 - 4\langle\cos^2[\gamma(t')]\rangle_{t'} + 4[(\langle\cos^2[\gamma(t')]\rangle_{t'})^2 + (\langle\cos[\gamma(t')]\sin[\gamma(t')]\rangle_{t'})^2]. \qquad \textbf{[S52]}$$

Using the ergodic hypothesis, the averages over all times in Eq. **S52** can be computed as averages over the ensemble of all possible values of the dihedral angles γ with the probability distribution $P(\gamma)$. The latter is related to the FEP by the Boltzmann formula:

$$P(\gamma) = \exp[-V(\gamma)/kT]. \qquad \textbf{[S53]}$$

Therefore, the order parameter S^2 of the dihedral angles γ were computed from the FEP $V(\gamma)$ by using the following formula:

$$S_\gamma^2 = \tilde{T}_2(\infty) = 1 - 4\langle\cos^2(\gamma)\rangle + 4[(\langle\cos^2(\gamma)\rangle)^2 + (\langle\cos(\gamma)\sin(\gamma)\rangle)^2], \quad \textbf{[S54]}$$

in which

$$\langle\,\rangle = \int_{-\pi}^{+\pi} d\gamma P(\gamma). \quad \textbf{[S55]}$$

8.2. Diffusion on a sphere (see Fig. S1). Using the following notations and the spherical coordinates θ and φ (Fig. S1),

$$\mathbf{u} = (u_x,u_y,u_z) \equiv \mathbf{u}(t') = (\sin[\theta(t')]\cos[\varphi(t')], \sin[\theta(t')]\sin[\varphi(t')], \cos[\theta(t')]), \quad \textbf{[S56]}$$

and

$$\bar{\mathbf{u}} = (\bar{u}_x,\bar{u}_y,\bar{u}_z) \equiv \mathbf{u}(t'+\infty) = (\sin[\theta(t'+\infty)]\cos[\varphi(t'+\infty)], \sin[\theta(t'+\infty)] \times \sin[\varphi(t'+\infty)], \cos[\theta(t'+\infty)]). \quad \textbf{[S57]}$$

the RCF (see Eq. **S8**) as $t \to \infty$ is

$$\tilde{P}_2(\infty) = \frac{3}{2}\langle(\bar{\mathbf{u}}\cdot\mathbf{u})^2\rangle - \frac{1}{2}, \quad \textbf{[S58]}$$

$$\tilde{P}_2(\infty) = \frac{3}{2}\langle\bar{u}_x{}^2u_x{}^2 + \bar{u}_y{}^2u_y{}^2 + \bar{u}_z{}^2u_z{}^2\rangle + 3\langle\bar{u}_x\bar{u}_yu_xu_y\rangle + 3\langle\bar{u}_x\bar{u}_zu_xu_z\rangle + 3\langle\bar{u}_z\bar{u}_yu_zu_y\rangle - \frac{1}{2}. \quad \textbf{[S59]}$$

By definition, the vectors $\bar{\mathbf{u}}$ and $\mathbf{u}$ are two orientations of the same vector separated by an infinite time. They are therefore statistically independent. Consequently, the average of their product is equal to the product of their averages. Using this property, we find

$$\tilde{P}_2(\infty) = \frac{3}{2}[\langle\bar{u}_x{}^2\rangle\langle u_x{}^2\rangle + \langle\bar{u}_y{}^2\rangle\langle u_y{}^2\rangle + \langle\bar{u}_z{}^2\rangle\langle u_z{}^2\rangle] + 3\langle\bar{u}_x\bar{u}_y\rangle\langle u_xu_y\rangle + 3\langle\bar{u}_x\bar{u}_z\rangle\langle u_xu_z\rangle + 3\langle\bar{u}_z\bar{u}_y\rangle\langle u_zu_y\rangle - \frac{1}{2}, \quad \textbf{[S60]}$$

and

$$\tilde{P}_2(\infty) = \frac{3}{2}[\langle u_x{}^2\rangle^2 + \langle u_y{}^2\rangle^2 + \langle u_z{}^2\rangle^2] + 3\langle u_xu_y\rangle^2 + 3\langle u_xu_z\rangle^2 + 3\langle u_zu_y\rangle^2 - \frac{1}{2}. \quad \textbf{[S61]}$$

Eq. **S61** follows from Eq. **S60** because a translation of the time scale by a constant (+∞) does not change the averages:

$$\langle\bar{u}_\alpha(t')\bar{u}_\beta(t')\rangle_{t'} = \langle u_\alpha(t'+\infty)u_\beta(t'+\infty)\rangle_{t'}, \quad \textbf{[S62]}$$

where $\alpha = x$ or y and $\beta = x$ or y.

Because $\mathbf{u}$ is an unit vector, one has

$$u_z{}^2 = 1 - u_x{}^2 - u_y{}^2. \quad \textbf{[S63]}$$

Using Eq. **S63** in Eq. **S61**, we find the following expression:

$$\tilde{P}_2(\infty) = 1 - 3\lfloor\langle u_x{}^2\rangle + \langle u_y{}^2\rangle\rfloor + 3[\langle u_x{}^2\rangle^2 + \langle u_y{}^2\rangle^2 + \langle u_x{}^2\rangle\langle u_y{}^2\rangle + \langle u_xu_y\rangle^2 + \langle u_xu_z\rangle^2 + \langle u_zu_y\rangle^2]. \quad \textbf{[S64]}$$

It is interesting to note that the sum of the first two terms in Eq. **S64** is similar to the *approximate* expression of the generalized parameter of a backbone N-H bond derived by Abergel and Bodenhausen in ref. 10 by assuming small displacements of the vector $\mathbf{u}$ relative to its average position. Approximation of small displacements (Δθ, Δφ) is, however, not fully justified (see, for example, the FEP in Fig. 1*B*, *Inset*, and Fig. 3*B* of the main text) in particular for the N-H bonds that exist in multiple substates [as, for example, $(\text{N-H})_{39}$]. The exact expression (**S64**) contains additional terms, which contribute to $\tilde{P}_2(t \to \infty)$ when the displacements are not small.

Finally, using the relation (**S56**), one finds

$$\begin{aligned}\tilde{P}_2(\infty) = 1 &- 3(\langle(\sin[\theta(t')]\cos[\varphi(t')])^2\rangle + \langle(\sin[\theta(t')]\sin[\varphi(t')])^2\rangle) \\ &+ 3(\langle(\sin[\theta(t')]\cos[\varphi(t')])^2\rangle^2 + \langle(\sin[\theta(t')]\sin[\varphi(t')])^2\rangle^2 \\ &+ \langle(\sin[\theta(t')]\cos[\varphi(t')])^2\rangle\langle(\sin[\theta(t')]\sin[\varphi(t')])^2\rangle \\ &+ \langle(\sin[\theta(t')])^2\cos[\varphi(t')]\sin[\varphi(t')]\rangle^2 \\ &+ \langle\sin[\theta(t')]\cos[\theta(t')]\cos[\varphi(t')]\rangle^2 \\ &+ \langle\sin[\theta(t')]\cos[\theta(t')]\sin[\varphi(t')]\rangle^2). \end{aligned} \quad \textbf{[S65]}$$

Using the ergodic hypothesis, the averages over time in Eq. **S65** can be computed as averages over the ensemble of all possible values of the polar angles θ and φ with the probability distribution $P(\theta,\varphi)$. The latter is related to the FEP by the Boltzmann formula:

$$P(\theta,\varphi) = \exp[-V(\theta,\varphi)/kT]. \quad \textbf{[S66]}$$

Therefore, the order parameters S^2 of the N-H bonds were computed from the FEP $V(\theta,\varphi)$ by using the following formula:

$$\begin{aligned}S_{\text{NH}}^2 = \tilde{P}_2(\infty) &= 1 - 3(\langle(\sin[\theta]\cos[\varphi])^2\rangle + \langle(\sin[\theta]\sin[\varphi])^2\rangle) \\ &+ 3(\langle(\sin[\theta]\cos[\varphi])^2\rangle^2 + \langle(\sin[\theta]\sin[\varphi])^2\rangle^2 \\ &+ \langle(\sin[\theta]\cos[\varphi])^2\rangle\langle(\sin[\theta]\sin[\varphi])^2\rangle \\ &+ \langle(\sin[\theta])^2\cos[\varphi]\sin[\varphi]\rangle^2 + \langle\sin[\theta]\cos[\theta]\cos[\varphi]\rangle^2 \\ &+ \langle\sin[\theta]\cos[\theta]\sin[\varphi]\rangle^2), \end{aligned} \quad \textbf{[S67]}$$

in which

$$\langle\,\rangle = \int_0^\pi d\theta \int_0^{2\pi} d\varphi P(\theta,\varphi). \quad \textbf{[S68]}$$

9. Application of the Model-Free Approach to the RCF of the N-H Bonds Computed from MD (Table S1 and Fig. S6). The "model-free" (MF) approach (11, 12) was applied to the RCFs of the backbone N-H bonds computed from MD. The MF approach is derived by assuming that the relaxation time of the overall tumbling of the whole protein [typically larger than 2 ns (13)] is much larger than the relaxation time of the motions of the N-H bonds (11–13). Under this assumption, $C_2(t)$ is represented as a linear interpolation between the limits, $C_2(0) = 1$ and $C_2(\infty) \equiv S^2$, i.e., (11–13)

$$C_2(t) = S^2 + [1 - S^2]f_2(t), \quad \textbf{[S69]}$$

where the function $f_2(t)$ describes the decay of the RCF as a function of the time and obeys $f_2(0) = 1$ and $f_2(\infty) = 0$. Generally, it is assumed that the RCF decays as an exponential (11),

$$f_2(t) = \exp(-t/\tau_f), \quad \textbf{[S70]}$$

which means a free rotational diffusion of $\boldsymbol{u}_n$ with a relaxation time τ_f (11).

The RCFs of the N-H bonds of VA3 computed by MD (run 1) up to 1 ns were fitted by using Eqs. **S69** and **S70**. The values of the parameters (S^2,τ_f) calculated for each residue are given in Table S1. For the N-H bonds moving in a single-minimum FEP, we find $0.64 < S^2 < 1$ and $\tau_f < 53$ ps, whereas, for N-H bonds existing in multiple substates (multiminima FEP), we find $S^2 < 0.8$ and 80 ps $< \tau_f <$ 530 ps [except $(\text{N-H})_2$, which has a multiminima FEP and a $\tau_f < 60$ ps). For N-H bonds existing in multiple substates (residues 2, 26, 37, 38, 39, and 40), we have also fitted the RCF computed by MD (run 1) up to 1 ns by using the multiexponential MF approach (12). The RCF was fitted by using Eq. **S69** and (see ref. 12)

$$f_2(t) = a_f \exp(-t/\tau_f) + (1 - a_f)\exp(-t/\tau_s), \qquad \textbf{[S71]}$$

with a_f a parameter weighting the fast motions and τ_s the relaxation time of a slow process [interpreted as the transitions between different stable orientations of the bonds (12)]. The values of S^2 using a monoexponential Eq. **S70** or biexponential Eq. **S71** model of the RCF are very similar as shown in Table S1. For the slow process, we find 170 ps $< \tau_s <$ 380 ps. Introduction of a slow process for bonds having multiminima FEP reduces the value of their relaxation time to $\tau_f < 8$ ps. The weight of the fast process, a_f, varies between 0.48 and 0.78. It is worth noting that the relaxation times found here are smaller than the typical tumbling relaxation time of a protein as required to apply the MF approach.

In order to compare the MF approach with the stretched exponential model used in the main paper, we develop expression **S71** at short time ($t \ll \tau_f$):

$$\begin{aligned} f_2(t) &\approx a_f(1 - t/\tau_f) + (1 - a_f)(1 - t/\tau_s) \\ &= 1 - \lfloor a_f/\tau_f + (1 - a_f)/\tau_s \rfloor t. \end{aligned} \qquad \textbf{[S72]}$$

Using Eq. **S72** in Eq. **S69**, we deduce

$$C_2(t) \approx 1 - (1 - S^2)(a_f/\tau_f + [1 - a_f]/\tau_s)t. \qquad \textbf{[S73]}$$

Comparing Eq. **S73** with Eq. **1** of the main text, we deduce an effective diffusion constant D_{MF} for the MF approach:

$$D_{\text{MF}} = \frac{1}{6}(1 - S^2)[a_f/\tau_f + (1 - a_f)/\tau_s]. \qquad \textbf{[S74]}$$

In the monoexponential MF approach ($a_f = 1$), the values of the effective diffusion constant at short time scale $t \ll \tau_f$ are much more smaller than the values of D_α (shown in Fig. S6*b*): D_{MF} varies between 2 deg^2/ps and 12 deg^2/ps (Table S1). Therefore, the values of the effective diffusion constant on a short time scale $t \ll \tau_f$ does not agree with the angular MSD of the N-H bonds, as expected because the MSD does not grow linearly with time as assumed in the MF approach and Eq. **S73**. For N-H bonds existing in multiple substates, the constants D_{MF} were also computed by using the biexponential model of $f_2(t)$ and their values are given in parentheses in Table S1. It is interesting to note that, for these residues, including a slow process, i.e., a multiexponential model of the RCF, increases the constant D_{MF} by an order of magnitude, similar to the one of D_α. This effect is due to the large decreases of τ_f in the biexponential model. It is worth noting that a stretched exponential decay can, in principle, be represented by an infinite sum of exponentials. Therefore, including additional exponentials in $f_2(t)$ brings the MF approach into better agreement with the stretched exponential decay that we observed in the RCF computed from MD.

Finally, the RCFs, computed from MD (run 1) up to 1 ns were also fitted with the MF approach by using Eq. **S69** and a stretched exponential model of the function $f_2(t)$, namely,

$$f_2(t) = \exp(-6At^\alpha), \qquad \textbf{[S75]}$$

where A and α are the two parameters fitted to the RCFs computed from MD. The parameter S^2 in Eq. **S69** was computed from the FEP by using Eq. **S67**. In order to compare this nonexponential MF approach with the stretched exponential model used in the main paper, we expand expression **S69** at short-time:

$$C_2(t) \approx S^2 + [1 - S^2)](1 - 6At^\alpha) = 1 - 6(1 - S^2)At^\alpha. \qquad \textbf{[S76]}$$

Comparing Eq. **S76** with Eq. **1** of the main text, we deduce an effective diffusion constant D_α, related to A and S^2:

$$D_\alpha \equiv A(1 - S^2). \qquad \textbf{[S77]}$$

The parameters α and D_α deduced from Eqs. **S69**, **S75**, and **S77** are compared to those deduced from the stretched exponential model discussed in the main text and fitted to the RCFs up to 1 ns in Fig. S6 *b* and *c* , respectively. The profile of D_α along the sequence of the amino acids calculated from the present nonexponential MF approach is similar to the one extracted from the MSD of the N-H bonds and from the stretched exponential model of the RCF's (Fig. S6*b*). The values of D_α deduced from Eq. **S77** are of the right order of magnitude but are in general much larger than the values deduced from the calculation of the MSD of the bonds. Similarly, the profile of the exponents deduced from the present nonexponential MF approach is only qualitatively similar to the one deduced from the MSD (Fig. S6*c*).

10. Materials and Methods. Five MD simulations of VA3, each of a duration of 80 ns, were carried out in explicit water [Simple Point Charge (SPC) force field] with the GROMACS package (14) and the all-atom Optimized Potentials for Liquid Simulations force field (15). The initial structure of VA3 was taken from one of the NMR models, model 1 (16). Six Cl^- counterions were used to neutralize VA3. The time step used was 2 fs, the temperature was set to 300 K, and the pressure to 1 bar by using a Berendsen thermostat and barostat (17), with coupling times of 0.1 and 1 ps, respectively. The protein was solvated in a triclinic box of 3002 SPC water molecules (18) keeping a minimum distance of 1 nm between the solute and each face of the box. The particle-mesh Ewald method (19, 20) was used for the calculation of long-range electrostatic interactions as it improves the accuracy of the force field compared to NMR data as shown recently (21); 0.9 nm was used for the van der Waals cutoff. Each MD simulation was carried out with different initial conditions for VA3 after 600-ps equilibrium time. The coordinates were saved every 1 ps. The steepest-descent algorithm with tolerance of 1,000 kJ/(mol nm) and maximum step size 0.01 nm implemented in GROMACS (11) was used for energy minimization.

Because of the presence of disulfide bonds, VA3 remains folded in all MD trajectories, which enables one to apply, with confidence, the separation of internal motions of the protein from its overall motion by aligning the MD snapshots on a reference structure. This procedure is required to define the orientation of the N-H bonds in a fixed molecular frame (reference structure) in order to compute their internal RCFs (11–13, 22) and their potential $V(\theta,\varphi)$. The calculation of RCFs of dihedral angles γ does not require aligning the MD snapshots because motion of the molecule as a whole does not affect the values of the γ angles.

1. Zwansig R, Ailawadi K (1969) Statistical error due to finite time averaging in computer experiments. *Phys Rev* 182:280–283.
2. Lu CY, Vanden Bout BA (2006) Effect of finite trajectory length on the correlation function analysis of single molecule data. *J Chem Phys* 125:124701.
3. Senet P, Maisuradze GG, Foulie C, Delarue P, Scheraga HA (2008) How main-chains of proteins explore the free-energy landscape in native states. *Proc Natl Acad Sci USA* 105:19708–19713
4. Vallée RAL, Paul W, Binder K (2007) Single molecule probing of the glass transition phenomenon: Simulations of several types of probes. *J Chem Phys* 127:154903
5. Perrin F (1928) Etude mathématique du mouvement Brownien de rotation. (Mathematical study of rotational Brownian motion) *Ann Sci Ecole Norm S* 45:1–51.
6. Abramowitz M, Stegun IA (1964) *Handbook of Mathematical Functions with Formulas, Graphs and Mathematical Tables* (Dover, New York), 9th Ed, Chap 22, pp 771–784.
7. McQuarrie DA (2000) *Statistical Mechanics* (University Science Books, Sausalito, CA), Chap 21, pp 512–522.
8. Lim SC, Muniandy SV (2002) Self-similar Gaussian process for modelling anomalous diffusion. *Phys Rev E* 66:021114.
9. Min W, Luo G, Cherayil BJ, Kou SC, Xie XS (2005) Observation of a power-law memory kernel for fluctuations within a single protein molecule. *Phys Rev Lett* 94:198302.
10. Abergel D, Bodenhausen G (2004) A simple model for NMR relaxation in the presence of internal motions with dynamical coupling. *J Chem Phys* 121:761–768.
11. Lipari G, Szabo A (1982) Model-free approach to the interpretation of nuclear magnetic resonance relaxation in macromolecules. 1. Theory and range of validity. *J Am Chem Soc* 104:4546–4559.
12. Clore GM, et al. (1990) Deviations from the simple two-parameter model-free approach to the interpretation of Nitrogen-15 nuclear magnetic relaxation of proteins. *J Am Chem Soc* 112:4989–4991.
13. Halle B (2009). The physical basis of model-free analysis of NMR relaxation data from proteins and complex fluids. *J Chem Phys* 131:224507.
14. Hess B, Cutzner C, van der Spoel D, Lindahl E (2008) GROMACS 4: Algorithms for highly efficient, load-balanced, and scalable molecular simulation. *J Chem Theory Comput* 4:435–447.
15. Jorgensen WL, Maxwell DS, Tirado-Rives J (1996) Development and testing of the OPLS all-atom force field on conformational energetics and properties of organic liquids. *J Am Chem Soc* 118:11225–11236.
16. Romagnoli S, et al. (2000) NMR structural determination of Viscotoxin A3 from Viscum album L. *Biochem J* 350:569–577.
17. Berendsen HJC, Postma JPM, van Gusteren WF, DiNola A, Haak JR (1984) Molecular dynamics with coupling to an external bath. *J Chem Phys* 81:3684–3690.
18. Berendsen HJC, Postma JPM, van Gusteren WF, Hermans J (1981) Interaction models for water in relation to protein hydration. *Intermolecular Forces*, ed Pullman B (Reidel, Dordrecht, The Netherlands), pp 331–342.
19. Darden T, York D, Pedersen L (1993) Particle mesh Ewald: An $N\cdot\log(N)$ method for Ewald sums in large systems. *J Chem Phys* 98:10089–10092.
20. Essmann U, et al. (1995) A smooth particle mesh Ewald method. *J Chem Phys* 103:8577–8593.
21. Lange OF, van der Spoel D, de Groot BL (2010) Scrutinizing molecular mechanics force fields on the submicrosecond timescale with NMR data. *Biophys J* 99:647–655.
22. Brüschweiler R (2003) New approaches to the dynamic interpretation and prediction of NMR relaxation data from proteins. *Curr Opin Struct Biol* 13:175–183.

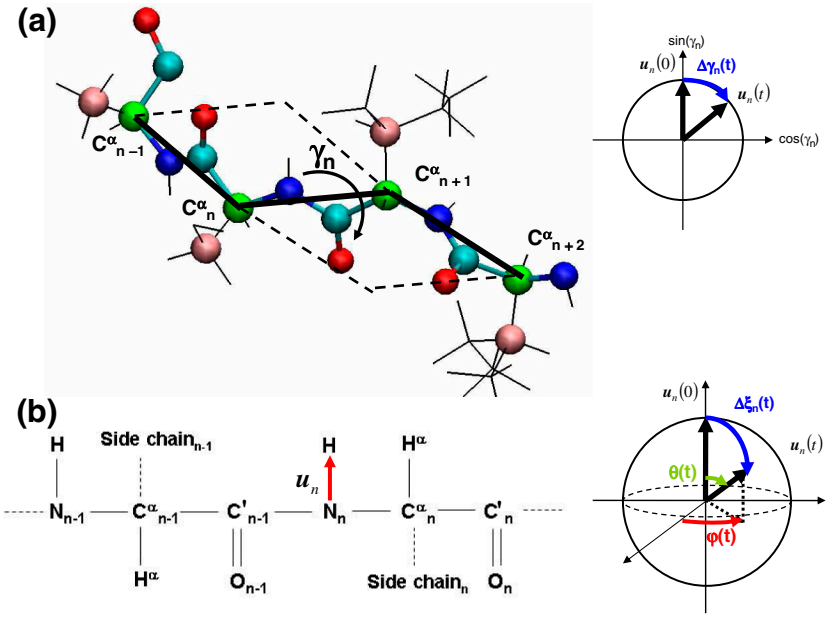

Fig. S1. (*a*) Definition of a coarse-grained dihedral angle γ_n constructed from four consecutive C^{α} atoms, and of the corresponding vector $\boldsymbol{u}_n$ and the angular displacement $\Delta\gamma_n$ on the unit circle. (*b*) Definition of the $(\text{N-H})_n$ bond and of the corresponding vector $\boldsymbol{u}_n$ and the angular displacement $\Delta\xi_n$ on the unit sphere. The polar coordinates θ and φ of the hydrogen atom of the $(\text{N-H})_n$ bond at time t are represented in colors on the unit sphere. For PRO residues, the displacements $\Delta\xi_n$ and the polar coordinates are not defined.

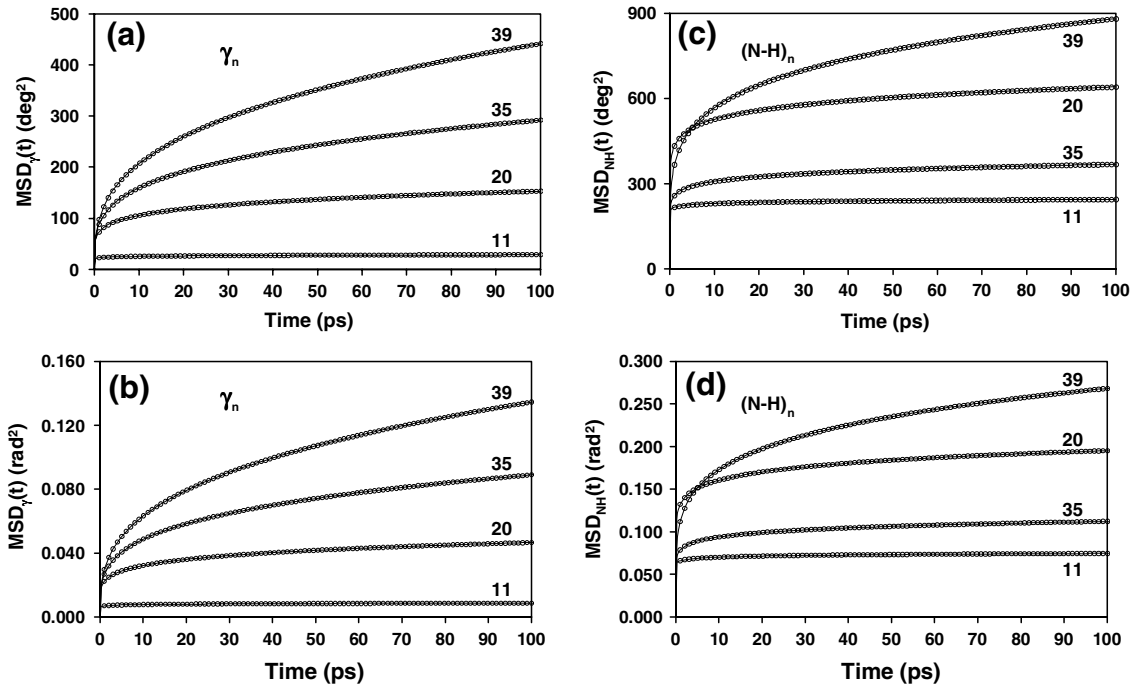

Fig. S2. Typical results for the MSD computed from MD (empty circles) of the dihedral angles γ_n (*a* and *b*) and of the $(N\text{-}H)_n$ bonds (*c* and *d*) at short time (t < 100 ps) in deg^2 (*a* and *c*) and in rad^2 (*b* and *d*). The MSD computed from MD were fitted up to 50 ps by power laws, namely, $MSD(t) = 2D_\alpha t^\alpha$ and $MSD(t) = 4D_\alpha t^\alpha$ for the dihedral angles γ_n and the $(N\text{-}H)_n$ bonds, respectively. The fits (thin lines) cannot be distinguished from the MD data at the scale of the figure.

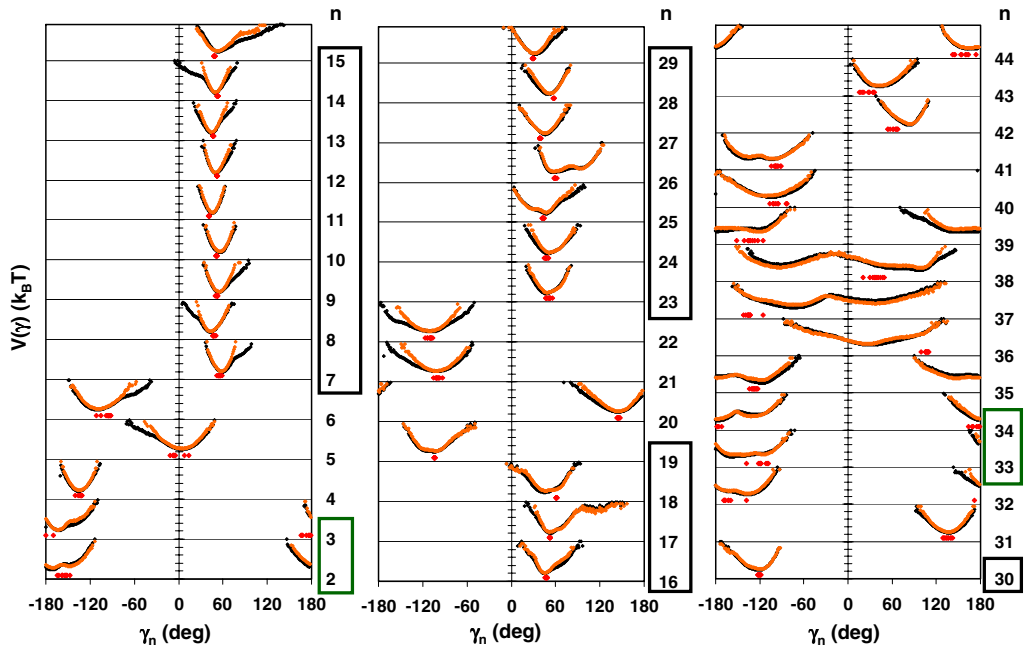

Fig. S3. Effective FEP $V(\gamma)$ of VA3 computed from MD along the primary sequence (γ_n, n = 2 to 44) compared to NMR-derived structural data (red diamonds) computed from the different models of VA3 in PDB ID code 1ED0 (ref. 16). The potentials $V(\gamma)$ were computed from five different MD runs of 80 ns each with different initial conditions by using the GROMACS force field and package. The first run (orange curve) out of the five runs is the one discussed in the paper. For comparison, the FEP averaged over five MD runs (black curve) is shown. Residues n located in a helix are in a black box and residues located in a β-sheet are in a green box.

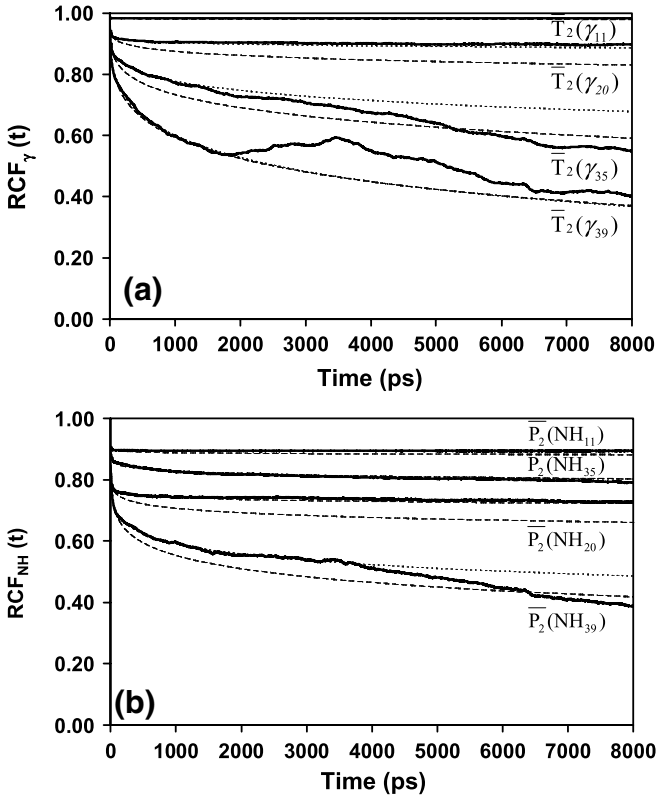

Fig. S4. (*a*) Typical results for RCF $\bar{T}_2$ of coarse-grained dihedral angles γ_n of VA3 computed from MD up to $t < 8$ ns. Results are presented for dihedral angles γ_{11}, γ_{20}, γ_{35}, and γ_{39} having free-energy profiles (shown schematically in Fig. 1*A*, *Inset*, of the main paper), representative of all $V(\gamma)$ calculated by MD (Fig. S3). For each dihedral angle γ_n, the RCF $\bar{T}_2$ (bold lines) is compared to two stretched exponentials (dashed and dotted lines) with an exponent α_n and diffusion constant D_α computed from a fit of RCF up to 50 ps (dashed lines) and from a fit up to 1 ns (dotted lines), respectively. (*b*) Typical results for long-time behavior ($t < 8$ ns) of RCF $\bar{P}_2$ of amide $(\text{N-H})_n$ bonds (Fig. S1) of VA3 computed from MD (data shown are for $n = 11$, 20, 35, and 39 from run 1). For each $(\text{N-H})_n$ bond associated with residue n, the RCF $\bar{P}_2$ (bold lines) is compared to two stretched exponentials (dashed and dotted lines) with an exponent α_n and diffusion constant D_α computed from a fit of RCF up to 50 ps (dashed lines) and from a fit up to 1 ns (dotted lines), respectively.

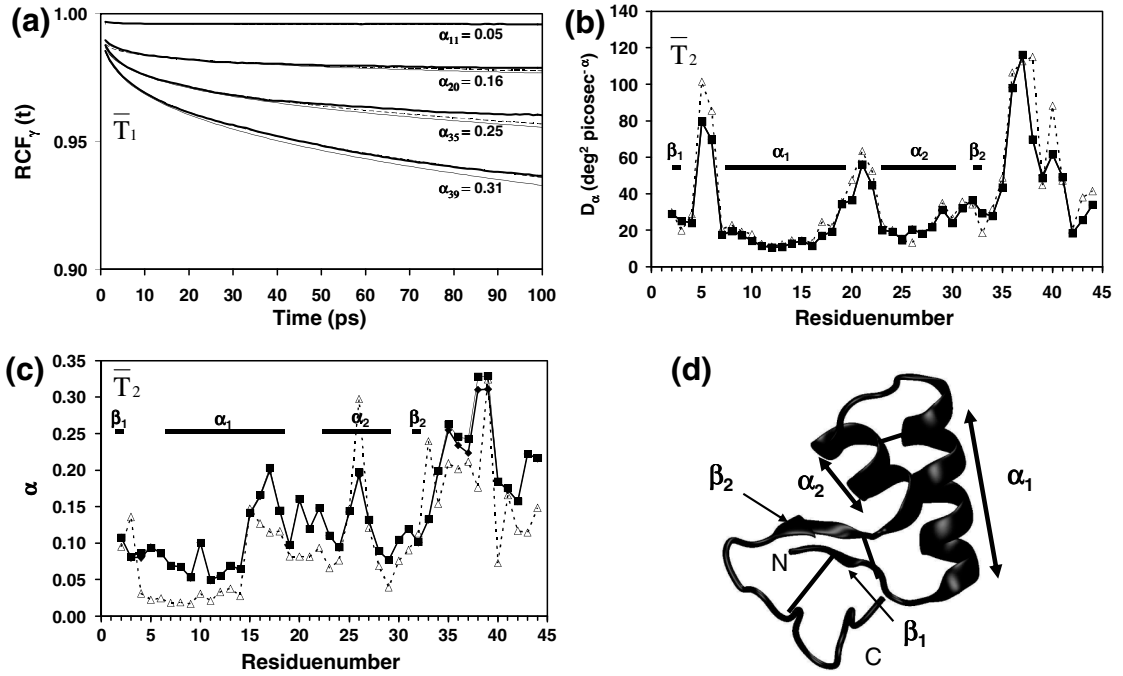

Fig. S5. (*a*) Typical results for RCFs of coarse-grained dihedral angles γ_n of VA3 computed from MD at t < 100 ps. For each dihedral angle γ_n, the RCF $\bar{T}_1$ (bold lines) is compared to Eq. **1** of the main text (thin lines) and to a stretched exponential $\exp(-D_\alpha t^\alpha)$ (dashed lines). In Eq. **1** of the main text, we used the $\mathrm{MSD}(t) = 2D_\alpha t^\alpha$ with an exponent α and the diffusion constant D_α computed by fitting the MSD up to 50 ps. The exponent α and a diffusion constant D_α of the stretched exponential were computed by fitting the RCF up to 50 ps. Exponents of the stretched exponential are given. The exponents computed by fitting the MSD are similar ($\alpha_{11} = 0.05$, $\alpha_{20} = 0.16$, $\alpha_{35} = 0.26$, $\alpha_{39} = 0.33$). The RCF computed using both Eq. **1** of the main text and the stretched exponential are hardly distinguishable for γ_{11} and γ_{20}. (*b*) Diffusion constants D_α along the primary sequence of VA3 computed by fitting RCF $\bar{T}_2$ of dihedral angles γ_n up to 50 ps by using a stretched exponential $\exp(-4D_\alpha t^\alpha)$ with an exponent α and diffusion constant D_α fitted to the RCF up to 50 ps (filled diamonds) and by using a stretched exponential $\exp(-4D_\alpha t^\alpha)$ with an exponent α and diffusion constant D_α fitted to the RCF up to 1 ns (empty triangles). Diffusion constants D_α calculated independently from a fit of the $\mathrm{MSD}(t)$ of γ_n by using $\mathrm{MSD}(t) \cong 2D_\alpha t^\alpha$ up to 50 ps (filled squares) overlap perfectly the parameters obtained from a fit of the RCF up to 50 ps by a stretched exponential (filled diamonds). Data are from trajectory 1 of VA3 and are representative of data obtained for all trajectories. (*c*) Exponents α along the primary sequence of VA3 computed by fitting RCF $\bar{T}_2$ of dihedral angles γ_n up to 50 ps by using a stretched exponential $\exp(-4D_\alpha t^\alpha)$ with an exponent α and diffusion constant D_α fitted to the RCF up to 50 ps (filled diamonds) and by using a stretched exponential $\exp(-4D_\alpha t^\alpha)$ with an exponent α and diffusion constant D_α fitted to the RCF up to 1 ns (empty triangles). Exponents α calculated independently from a fit of the $\mathrm{MSD}(t)$ of γ_n by using $\mathrm{MSD}(t) \cong 2D_\alpha t^\alpha$ up to 50 ps (filled squares) overlap perfectly the parameters obtained from a fit of the RCF up to 50 ps by a stretched exponential (filled diamonds) except for *n* between 35 and 39. Data are from trajectory 1 of VA3 and are representative of data obtained for all trajectories. (*d*) Main structural elements of VA3 (β-sheets β_1/β_2, helices α_1/α_2, and the straight solid lines showing the positions of the three disulfide bonds).

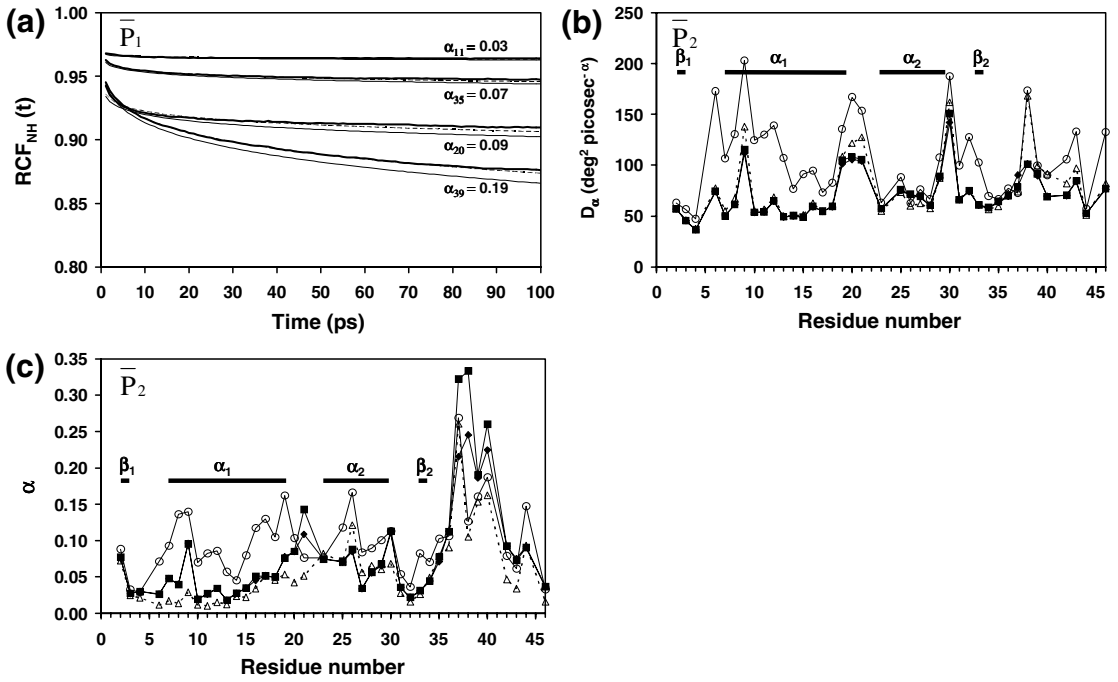

Fig. S6. Typical results for RCFs of $(\text{N-H})_n$ bonds of VA3 computed from MD at $t < 100$ ps. For each $(\text{N-H})_n$ bond, the RCF $\bar{P}_1$ (bold lines) is compared to Eq. **1** of the main text (thin lines) and to a stretched exponential $\exp(-2D_\alpha t^\alpha)$ (dashed lines). In Eq. **1** of the main text, we use $\text{MSD}(t) = 4D_\alpha t^\alpha$ with an exponent α and a diffusion constant D_α computed by fitting the MSD up to 50 ps. The exponent α and diffusion constant D_α of the stretched exponential were computed by fitting the RCF up to 50 ps. Exponents of the stretched exponential are given. The exponents computed by fitting the MSD are similar ($\alpha_{11} = 0.03$, $\alpha_{20} = 0.09$, $\alpha_{35} = 0.08$, $\alpha_{39} = 0.19$). The RCF computed using Eq. **1** of the main text and the stretched exponential are hardly distinguishable for $(\text{N-H})_{11}$, $(\text{N-H})_{35}$, and $(\text{N-H})_{39}$. (*b*) Diffusion constants D_α along the primary sequence of VA3 computed by fitting RCF $\bar{P}_2$ of $(\text{N-H})_n$ bonds up to 50 ps by using a stretched exponential $\exp(-6D_\alpha t^\alpha)$ with an exponent α and diffusion constant D_α fitted to the RCF up to 50 ps (filled diamonds) and by using a stretched exponential $\exp(-6D_\alpha t^\alpha)$ with an exponent α and diffusion constant D_α fitted to the RCF up to 1 ns (empty triangles). Diffusion constants D_α calculated independently from a fit of the MSD(t) of γ_n by using $\text{MSD}(t) \cong 4D_\alpha t^\alpha$ up to 50 ps (filled squares) nearly perfectly overlap the parameters obtained from a fit of the RCF up to 50 ps by a stretched exponential (filled diamonds) for most of the residues (see *SI Text*). Data are from trajectory 1 of VA3 and are representative of data obtained for all trajectories. The RCFs $\bar{P}_2$ computed from MD were also fitted up to 1 ns by using the model-free approach with a nonexponential function Eqs. **S69** and **S75** and a parameter S^2 computed from the FEP (Eq. **S67**). The parameters $D_\alpha \equiv A(1 - S^2)$ Eq. **S77** are shown (empty circles). (*c*) Exponents α along the primary sequence of VA3 computed by fitting RCF $\bar{P}_2$ of $(\text{N-H})_n$ bonds up to 50 ps by using a stretched exponential $\exp(-6D_\alpha t^\alpha)$ with an exponent α and diffusion constant D_α fitted on the RCF up to 50 ps (filled diamonds) and by using a stretched exponential $\exp(-6D_\alpha t^\alpha)$ with an exponent α and diffusion constant D_α fitted on the RCF up to 1 ns (empty triangles). Exponents α calculated independently from a fit of the MSD(t) of $(\text{N-H})_n$ bonds by using $\text{MSD}(t) \cong 4D_\alpha t^\alpha$ up to 50 ps (filled squares) overlap nearly perfectly the parameters obtained from a fit of the RCF up to 50 ps by a stretched exponential (filled diamonds) for most of the residues (see *SI Text*). Data are from trajectory 1 of VA3 and are representative of data obtained for all trajectories. The RCFs $\bar{P}_2$ computed from MD were also fitted up to 1 ns by using the model-free approach with a nonexponential function Eqs. **S69** and **S75** and a parameter S^2 computed from the FEP Eq. **S67**. The parameters α are shown (empty circles).

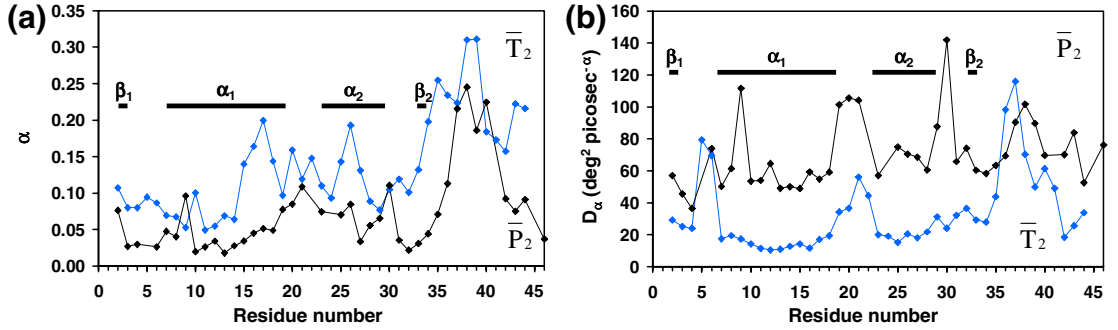

Fig. S7. Exponent α_n (*a*) and diffusion constant D_α (*b*) of amide $(\text{N-H})_n$ bonds (Fig. S1) along primary sequence of VA3 computed by fitting RCF $\bar{P}_2$ up to 50 ps by using a stretched exponential, namely, $\exp(-6D_\alpha t^\alpha)$ (black diamonds). Data are presented for run 1. For comparison, the exponents α_n (*a*) and the diffusion constant D_α (*b*) of the coarse-grained dihedral angles γ_n along the primary sequence of VA3 computed from run 1 by fitting RCF $\bar{T}_2$ up to 50 ps by using a stretched exponential, namely, $\exp(-4D_\alpha t^\alpha)$ are shown (blue diamonds). β_1/β_2 and α_1/α_2 are the locations of the two β-sheets and the two α-helices of VA3, respectively.

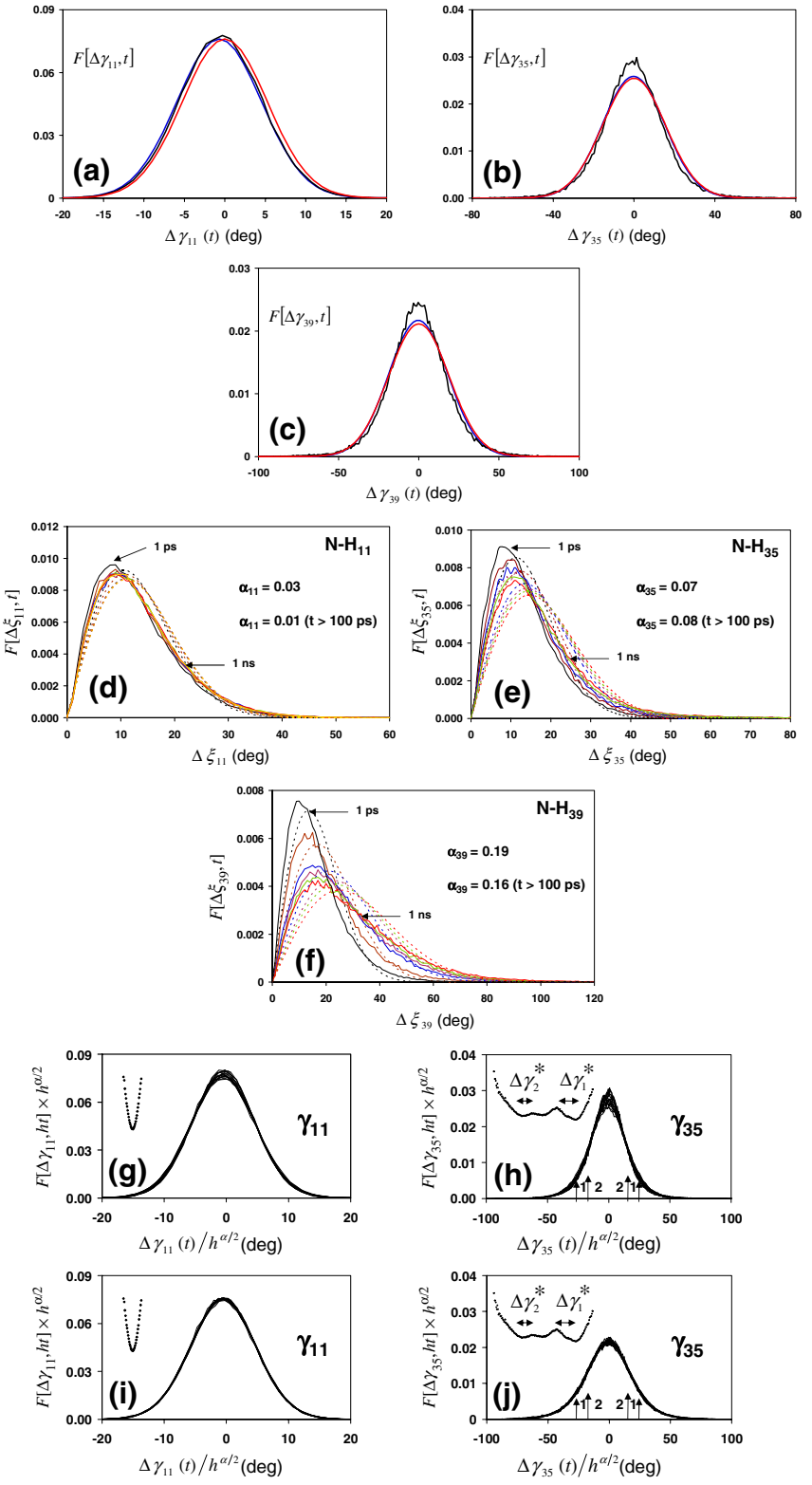

Fig. S8. (*a*–*c*) PDF $F(\Delta\gamma_n;t)$ of VA3 at $t = 50$ ps computed for the whole MD trajectory (run 1) (black line) and evaluated from Eq. **S17** (red line) and from Eq. **S30** with the sole term $k = 0$ (Gaussian PDF, blue line) with the parameters α and D_α of a stretched exponential fitted on $\bar{T}_2$ up to 50 ps. Results are presented for γ_{11} (*a*) with a typical harmonic FEP and for γ_{35} (*b*) and γ_{39} (*c*) with a typical multiple-minima FEP (see Fig. S3). (*d*–*f*) PDF $F(\Delta\xi_n;t)$ of VA3 computed for the whole MD trajectory (run 1) (full lines) and evaluated from Eqs. **S24** and **S26** (dashed lines) with the parameters α and D_α of a stretched exponential fitted to $\bar{P}_2$ over a duration of 50 ps for $t \leq 100$ ps and over a duration of 1 ns for $t > 100$ ps. Results are presented for $(\text{N-H})_{11}$ (*d*), for $(\text{N-H})_{35}$ (e), and for $(\text{N-H})_{39}$ (*f*) for $t = 1$ ps (black lines), 10 ps (brown lines), 100 ps (blue lines), 300 ps (purple lines), 500 ps (green lines), and for $t = 1$ ns (red lines). Note that some deviations at large times between the PDF computed in MD and Eqs. **S24** and **S26** were observed for residues with multiple-minima free-energy profiles as illustrated for $(\text{N-H})_{39}$ (*f*). (*g*–*j*) Typical results for the time evolution of the PDF of $\Delta\gamma_n$ computed from the fluctuations of γ_n extracted from MD trajectories of VA3. Results are presented for γ_{11} (*g* and *i*) with a typical harmonic FEP (*g*, *Inset*, and *i*, *Inset*), γ_{35} (*h* and *j*) with typical multiple-minima FEP (*h*, *Inset*, and *j*, *Inset*). In all panels, the

superposed curves are the PDFs computed from MD and rescaled by using Eq. **S34** at times $t = 10$, 20, 30, 40, 50, 60, 70, 80, 90, 100, 300, 500, 600, 800, and 1,000 ps (the maximum value of the PDF increases with time). (*g* and *h*) PDFs are rescaled by choosing $h = 1$ (Eq. **S34**) at $t = 100$ ps and an exponent α calculated from a fit to a stretched exponential of $\bar{T}_2$ up to 50 ps. (*i* and *j*) The PDFs are rescaled by choosing $h = 1$ (Eq. **S34**) at $t = 1$ ns and an exponent α calculated from a fit of $\bar{T}_2$ up to 1 ns. (*i* and *j*) The PDFs cannot be distinguished at the scale of the figure. (*h*, *Inset*, and *j*, *Inset*) ${\Delta\gamma_1}^*$ (${\Delta\gamma_2}^*$) represents the distance between the deepest minimum (a local minima) of the FEP and the nearest activation barrier; the distances ${\Delta\gamma_1}^*$ (${\Delta\gamma_2}^*$) are shown as arrows on the corresponding $\Delta\gamma$ axis.

Table S1. Parameters of the model-free approach (11, 12) fitted on the RCF $\bar{P}_2$ computed from MD up to 1 ns

Model-free approach of the RCF (11, 12): $C_2(t) = S^2 + (1 - S^2)f_2(t)$

$f_2(t) = \exp(-t/\tau_f)$			$f_2(t) = a_f \exp(-t/\tau_f) + (1 - a_f)\exp(-t/\tau_s)$				
Residue	S^2	τ_f (ps)	S^2	a_f	τ_f (ps)	τ_s (ps)	D_{MF} (deg^2 /ps)
2	0.85	34.48	0.84	0.78	0.79	342.50	2.38 (86.49)
3	0.91	11.17					4.41
4	0.93	12.28					3.12
6	0.86	6.30					12.16
7	0.89	11.17					5.39
8	0.88	8.39					7.83
9	0.74	14.36					9.91
10	0.90	6.30					8.68
11	0.90	7.63					7.17
12	0.87	6.93					10.26
13	0.91	6.93					7.11
14	0.90	10.15					5.39
15	0.90	12.28					4.46
16	0.87	21.76					3.27
17	0.87	26.33					2.70
18	0.87	23.94					2.97
19	0.76	21.76					6.03
20	0.75	19.78					6.92
21	0.73	22.00					6.71
23	0.85	39.81					2.06
25	0.81	29.39					3.54
26	0.79	85.24	0.77	0.67	0.85	380.05	1.35 (99.30)
27	0.85	19.78					4.15
28	0.86	28.97					2.64
29	0.80	19.84					5.52
30	0.64	22.81					8.64
31	0.87	10.15					7.01
32	0.86	6.30					12.16
33	0.88	11.17					5.88
34	0.87	21.76					3.27
35	0.84	32.41					2.70
36	0.80	47.23					2.32
37	0.49	522.09	0.44	0.48	2.82	313.37	0.53 (52.66)
38	0.56	89.92	0.54	0.75	4.76	170.42	2.68 (40.02)
39	0.63	164.44	0.59	0.65	3.90	363.77	1.23 (37.60)
40	0.63	229.60	0.60	0.64	7.22	300.03	0.88 (19.66)
42	0.82	26.50					3.72
43	0.81	17.99					5.78
44	0.85	52.29					1.57
46	0.85	7.6					10.80